XLI CILAMCE
XLI Ibero-Latin American Congress on Computational Methods in Engineering
16-19 November, 2020 FOZ DO IGUAÇU PARANÁ - BRAZIL

Smooth Second-Order Sliding Mode Flight Control of an Ellipsoidal Multirotor Airship

Jorge A. Ricardo Jr[1], Davi A. Santos [2]

[1] *Mr. Ricardo Jr is a PhD student in the Department of Mechatronics, Aeronautics Institute of Technology, São José dos Campos, SP, 12228-900, Brazil* jorgejarj@ita.br.
[2] *Dr. Santos is Associate Professor of the Department of Mechatronics, Aeronautics Institute of Technology, São José dos Campos, SP, 12228-900, Brazil* davists@ita.br.

Abstract. This work is concerned with the robust attitude and position tracking control of a multirotor airship subject to a smooth model uncertainty representing unknown aerodynamics coefficients and added mass. The vehicle is assumed to be full-actuated. To tackle this problem, we present a multi-input formulation of a smooth second-order sliding mode control strategy with stability guaranteed on the basis of vector field homogeneity. The method is evaluated using numerical simulation and shows effective.

Keywords: Sliding mode control, multirotor airship, flight control, function homogeneity.

1 Introduction

The multirotor aerial vehicles (MAVs) have become popular in applications such as surveillance [1], object delivery [2], and agriculture monitoring [3]. In all the cited applications, the flight mission effectiveness and efficiency could be increased if the flight duration and payload capability were extended. A simple and effective way to improve those characteristics in MAVs is to combine them with an aerostatic balloon, filled with helium, for example, giving rise to a multirotor airship [4, 5].

It turns out that the flight dynamics of a multirotor airship, besides of being very coupled and nonlinear, are susceptible to variability of environmental conditions [5] as well as to aerodynamic effects, which are difficult to predict precisely [6]. For this reason, a multivariable robust design approach would be a suitable choice for obtaining its flight control laws.

The sliding mode control (SMC) [7] is a variable structure control (VSC) method that emerged in the early 1950s in the Soviet Union with Emelyanov [8] and his co-researches Itkis [9] and Utkin [10]. It is one of the most effective control methods for systems under bounded matched uncertainties/disturbance [11]. The general idea of the conventional (first-order) SMC is to adopt a switching feedback control to steer and keep the system states on a manifold of the state space, where it becomes governed by a desired reduced dynamic model which is not affected by the uncertainties/disturbance. However, due to actuator latency, in practice, it suffers from chattering and, consequently, does not result in the designed performance [12]. The conventional SMC is restricted to systems with output relative-degree of 1. Fortunately, it has been extended to the high-order sliding mode (HOSM), which removes the relative-degree restriction and, in practice, can almost eliminate the chattering [13]. A special class of HOSM controllers that can also avoid chattering and has already been successfully implemented in real problems [14–16] is the so-called second-order sliding mode control (2-SMC).

In this context, the present paper extends the single-input smooth 2-SMC proposed by Shtessel et al. [16] into a multi-input formulation, which is then applied to the control of a full-actuated multirotor airship with six degrees of freedom (DOF). For the sake of simplicity, in the present study, the specific rotor configuration as well as the actuator dynamic modeling are not considered. Thus, the paper tackles a specific part of a broader control problem, which encompass the control allocation into the rotors configuration and its subsequently application to the complete vehicle's dynamics.

The remaining text is organized as follows. Section 2 presents a flight dynamic modeling for the multirotor airship, defines the error dynamics, and details the control objective. Section 3 designs the multi-input smooth 2-SMC law for position and attitude control. Section 4 presents the results of the

numerical simulations. Section 5 concludes the paper.

2 Problem Definition

Subsection 2.1 presents the adopted notation. Subsection 2.2 describes the vehicle's dynamics. Subsection 2.3 presents the error dynamics. Lastly, Subsection 2.4 states the control objective.

2.1 Notation

Matrices and algebraic vectors are denoted, respectively, by uppercase and lowercase boldface letters. On the other hand, physical vectors are denoted as in $\vec{a}$. An arbitrary Cartesian coordinate system (CCS) is denoted by $\mathcal{S}_b \triangleq \{B; \vec{x}_b, \vec{y}_b, \vec{z}_b\}$, with B representing its origin, and $\vec{x}_b$, $\vec{y}_b$, and $\vec{z}_b$ its orthogonal unit vectors. The algebraic vectors corresponding to the projection of an arbitrary physical vector $\vec{a}$ onto $\mathcal{S}_b$ and $\mathcal{S}_g$ are denoted by $\mathbf{a}_b \in \mathbb{R}^3$ and $\mathbf{a}_g \in \mathbb{R}^3$, respectively. The relation between $\mathbf{a}_g$ and $\mathbf{a}_b$ is $\mathbf{a}_b = \mathbf{D}^{b/g}\mathbf{a}_g$, where $\mathbf{D}^{b/g} \in \mathrm{SO}(3)$ is the attitude matrix of $\mathcal{S}_b$ w.r.t. $\mathcal{S}_g$. The inverse of $\mathbf{D}^{b/g}$, which coincides with its transpose, is denoted by $\mathbf{D}^{g/b}$. The symbol $\mathbf{I}_n \in \mathbb{R}^{n\times n}$ denotes an identity matrix. The $n \times m$ zero matrix is denoted by $\mathbf{0}_{n\times m}$. The n dimensional one vector is denoted by $\mathbf{1}_n$. The standard unit vectors are denoted by $\mathbf{e}_1 \triangleq (1,0,0)$, $\mathbf{e}_2 \triangleq (0,1,0)$, and $\mathbf{e}_3 \triangleq (0,0,1)$. Let $\vec{a}^{\,b/g}$ represent a relative physical quantity of $\mathcal{S}_b$ relative to $\mathcal{S}_g$, *e.g.*, $\vec{r}^{\,b/g}$ denotes the (relative) position of $\mathcal{S}_b$ w.r.t. $\mathcal{S}_g$. Finally, consider the $\mathcal{S}_g$ representations $\mathbf{a}_g \triangleq (a_1, a_2, a_3)$ and $\mathbf{b}_g$ of $\vec{a}$ and $\vec{b}$, respectively. The vector product $\vec{c} = \vec{a} \times \vec{b}$ is represented in the same CCS by $\mathbf{c}_g = [\mathbf{a}_g\times]\mathbf{b}_g$, where $[\mathbf{a}_g\times]$ is the following skew-symmetric matrix:

$$[\mathbf{a}_g\times] \triangleq \begin{bmatrix} 0 & -a_3 & a_2 \\ a_3 & 0 & -a_1 \\ -a_2 & a_1 & 0 \end{bmatrix}.$$

2.2 Multirotor Airship Dynamics

Figure 1 illustrates an arbitrary multirotor airship as well as the adopted CCSs. The body CCS $\mathcal{S}_b \triangleq \{B; \vec{x}_b, \vec{y}_b, \vec{z}_b\}$ is located at the hull's center of volume, with $\vec{x}_b$ and $\vec{z}_b$ pointing frontward and upward, respectively. The ground CCS $\mathcal{S}_g \triangleq \{G; \vec{x}_g, \vec{y}_g, \vec{z}_g\}$ is fixed to the ground at a known point with $\vec{z}_g$ pointing upward vertically. Finally, the CCS $\mathcal{S}_c \triangleq \{C; \vec{x}_c, \vec{y}_c, \vec{z}_c\}$ is parallel to $\mathcal{S}_b$, but displaced to the vehicle's center of mass.

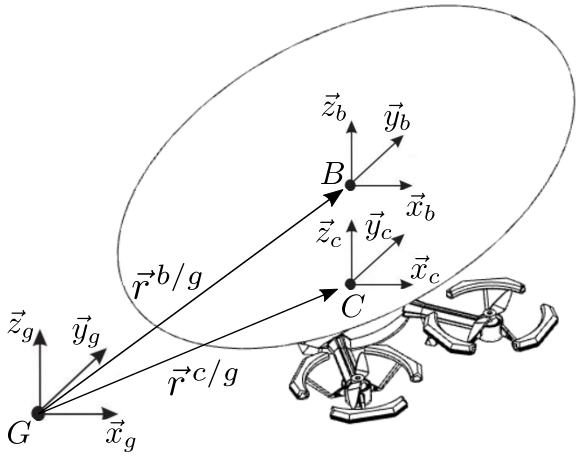

Figure 1. An illustrative multirotor airship and the adopted coordinate systems.

The position-attitude kinematics of $\mathcal{S}_b$ w.r.t. $\mathcal{S}_g$ are described by [6]:

$$\dot{\boldsymbol{\eta}} = \mathbf{A}(\boldsymbol{\eta})\,\boldsymbol{\nu}, \tag{1}$$

where $\boldsymbol{\eta} \triangleq (\mathbf{r}_g^{b/g}, \boldsymbol{\gamma}^{b/g})$, $\mathbf{r}_b^{b/g} \in \mathbb{R}^3$ is the position, $\boldsymbol{\gamma}^{b/g} \triangleq (\phi, \theta, \psi)$ are the 1-2-3 Euler angles, $\boldsymbol{\nu} \triangleq (\mathbf{v}_b^{b/g}, \boldsymbol{\omega}_b^{b/g})$, $\mathbf{v}_g^{b/g} \in \mathbb{R}^3$ is the linear velocity, $\boldsymbol{\omega}_b^{b/g} \in \mathbb{R}^3$ is the angular velocity,

$$\mathbf{A}(\boldsymbol{\eta}) \triangleq \begin{bmatrix} \mathbf{I}_3 & \mathbf{0}_{3\times3} \\ \mathbf{0}_{3\times3} & \mathbf{E}\left(\boldsymbol{\gamma}^{b/g}\right) \end{bmatrix} \in \mathbb{R}^{6\times6}, \tag{2}$$

$$\mathbf{E}\left(\boldsymbol{\gamma}^{b/g}\right) \triangleq \begin{bmatrix} \cos(\psi)/\cos(\theta) & -\sin(\psi)/\cos(\theta) & 0 \\ \sin(\psi) & \cos(\psi) & 0 \\ -\cos(\psi)\tan(\theta) & \sin(\psi)\tan(\theta) & 1 \end{bmatrix}. \tag{3}$$

On the other hand, the position-attitude dynamics of the airship are described by [6]:

$$\mathbf{M}(\boldsymbol{\eta})\,\dot{\boldsymbol{\nu}} + \mathbf{C}(\boldsymbol{\eta}, \boldsymbol{\nu})\,\boldsymbol{\nu} = \mathbf{P}(\boldsymbol{\eta})\,\boldsymbol{\tau}^c + \boldsymbol{\tau}^b + \boldsymbol{\tau}^g + \boldsymbol{\tau}^d, \tag{4}$$

where $\boldsymbol{\tau}^c \in \mathbb{R}^6$, $\boldsymbol{\tau}^b \in \mathbb{R}^6$, $\boldsymbol{\tau}^g \in \mathbb{R}^6$, and $\boldsymbol{\tau}^d \in \mathbb{R}^6$ are bounded and smooth force-torque vectors stemming from the control, aerostatic balloon, gravity, and disturbance, respectively. The effort vectors have their force and torque components represented in $\mathcal{S}_g$ and $\mathcal{S}_b$, respectively. The dynamic matrices are given by

$$\mathbf{M}(\boldsymbol{\eta}) \triangleq \begin{bmatrix} m\mathbf{I}_3 & -m\mathbf{D}^{g/b}\left[\mathbf{r}_b^{c/b}\times\right] \\ m\left[\mathbf{r}_b^{c/b}\times\right]\mathbf{D}^{b/g} & \mathbf{J}_b \end{bmatrix} \in \mathbb{R}^{6\times6}, \tag{5}$$

$$\mathbf{C}(\boldsymbol{\eta}, \boldsymbol{\nu}) \triangleq \begin{bmatrix} \mathbf{0}_{3\times3} & -m\mathbf{D}^{g/b}\left[\boldsymbol{\omega}_b^{b/g}\times\right]\left[\mathbf{r}_b^{c/b}\times\right] \\ \mathbf{0}_{3\times3} & -\left[\mathbf{J}_b\boldsymbol{\omega}_b^{b/g}\times\right] \end{bmatrix} \in \mathbb{R}^{6\times6}, \tag{6}$$

$$\mathbf{P}(\boldsymbol{\eta}) \triangleq \begin{bmatrix} \mathbf{I}_3 & \mathbf{0}_{3\times3} \\ \left[\mathbf{r}_b^{c/b}\times\right]\mathbf{D}^{b/g} & \mathbf{I}_3 \end{bmatrix} \in \mathbb{R}^{6\times6}, \tag{7}$$

with $m \in \mathbb{R}$ representing the total mass, $\mathbf{J}_b \in \mathbb{R}^{3\times3}$ the inertia matrix, and $\mathbf{r}_b^{c/b} \in \mathbb{R}^3$ the position of C w.r.t. B.

In particular, we adopt the following models for $\boldsymbol{\tau}^b$ and $\boldsymbol{\tau}^g$:

$$\boldsymbol{\tau}^b = \begin{bmatrix} \rho_{\text{air}} V^b g \mathbf{e}_3 \\ \mathbf{0}_{3\times1} \end{bmatrix}, \tag{8}$$

$$\boldsymbol{\tau}^g = \begin{bmatrix} -mg\mathbf{e}_3 \\ -m\left[\mathbf{r}_b^{c/b}\times\right]\mathbf{D}^{b/g} g\mathbf{e}_3 \end{bmatrix}, \tag{9}$$

where $\rho_{\text{air}} \in \mathbb{R}$ is the air density, $g \in \mathbb{R}$ is the gravity acceleration, and $V^b \in \mathbb{R}$ is the volume of the hull.

In Ricardo Jr [6], a computational fluid dynamics (CFD) model is developed for the drag, lift, and moment aerodynamic coefficients and a theoretic equation is formulated for the added mass. However, such aerodynamic effects on the multirotor airship are difficult to predict precisely for each particular situation due to parametric errors. For this reason, the current paper assumes that the respective efforts are comprised by $\boldsymbol{\tau}^d$.

2.3 Control Objective

Define the tracking control errors $\tilde{\boldsymbol{\eta}} \triangleq \bar{\boldsymbol{\eta}} - \boldsymbol{\eta}$ and $\tilde{\boldsymbol{\nu}} \triangleq \bar{\boldsymbol{\nu}} - \boldsymbol{\nu}$, with $\bar{\boldsymbol{\eta}}$ and $\bar{\boldsymbol{\nu}}$ representing the pose and velocity commands, respectively. The error kinematics and dynamics can be written as

$$\dot{\tilde{\boldsymbol{\eta}}} = \mathbf{A}(\boldsymbol{\eta})\,\tilde{\boldsymbol{\nu}}, \tag{10}$$

$$\dot{\tilde{\boldsymbol{\nu}}} = \mathbf{M}^{-1}(\boldsymbol{\eta})\left(\mathbf{C}(\boldsymbol{\eta}, \boldsymbol{\nu})\,\bar{\boldsymbol{\nu}} - \mathbf{C}(\boldsymbol{\eta}, \boldsymbol{\nu})\,\tilde{\boldsymbol{\nu}} - \boldsymbol{\tau}^b - \boldsymbol{\tau}^g - \mathbf{P}(\boldsymbol{\eta})\,\boldsymbol{\tau}^c - \boldsymbol{\tau}^d\right) + \dot{\bar{\boldsymbol{\nu}}}, \tag{11}$$

which can be expressed in the following canonical form

$$\dot{\mathbf{x}}_1 = \mathbf{f}_1(\mathbf{x}_1, \mathbf{x}_2), \tag{12}$$

$$\dot{\mathbf{x}}_2 = \mathbf{f}_2(\mathbf{x}_1, \mathbf{x}_2) + \mathbf{B}(\mathbf{x}_1)\mathbf{u} + \mathbf{G}(\mathbf{x}_1)\mathbf{d}, \tag{13}$$

by defining $\mathbf{x}_1 \triangleq \tilde{\boldsymbol{\eta}}$, $\mathbf{x}_2 \triangleq \tilde{\boldsymbol{\nu}}$, $\mathbf{u} \triangleq \boldsymbol{\tau}^c$, $\mathbf{d} \triangleq \boldsymbol{\tau}^d$, $\mathbf{B}(\mathbf{x}_1) \triangleq -\mathbf{M}^{-1}(\boldsymbol{\eta})\,\mathbf{P}(\boldsymbol{\eta})$, $\mathbf{G}(\mathbf{x}_1) \triangleq -\mathbf{M}^{-1}(\boldsymbol{\eta})$, $\mathbf{f}_1(\mathbf{x}_1, \mathbf{x}_2) \triangleq \mathbf{A}(\boldsymbol{\eta})\,\tilde{\boldsymbol{\nu}}$, and

$$\mathbf{f}_2(\mathbf{x}_1, \mathbf{x}_2) \triangleq \mathbf{M}^{-1}(\boldsymbol{\eta})\,\mathbf{C}(\boldsymbol{\eta}, \boldsymbol{\nu})\,\bar{\boldsymbol{\nu}} - \mathbf{M}^{-1}(\boldsymbol{\eta})\,\mathbf{C}(\boldsymbol{\eta}, \boldsymbol{\nu})\,\tilde{\boldsymbol{\nu}} - \mathbf{M}^{-1}(\boldsymbol{\eta})\left(\boldsymbol{\tau}^b + \boldsymbol{\tau}^g\right) + \dot{\bar{\boldsymbol{\nu}}}.$$

Now, define a sliding variable $\boldsymbol{\sigma} \in \mathbb{R}^6$:

$$\boldsymbol{\sigma} = \mathbf{f}_1(\mathbf{x}_1, \mathbf{x}_2) + \boldsymbol{\mathcal{C}}_{\boldsymbol{\sigma}}\mathbf{x}_1, \tag{14}$$

where $\boldsymbol{\mathcal{C}}_{\boldsymbol{\sigma}} \in \mathbb{R}^{6\times 6}$ is a diagonal parameter matrix.

The set $\boldsymbol{\sigma} = \mathbf{0}$ defines the sliding manifold corresponding to the sliding variable (14). It turns out that the dynamics of system (12)–(13) is collapsed to the reduced-order dynamics $\dot{\mathbf{x}}_1 = -\boldsymbol{\mathcal{C}}_{\boldsymbol{\sigma}}\mathbf{x}_1$.

Lemma 1. The sliding manifold reduced-order dynamics is asymptotically stable iff $\boldsymbol{\mathcal{C}}_{\boldsymbol{\sigma}}$ is positive definite.

Problem 1. The problem is to design a smooth control law for system (12)–(13) for attracting $(\boldsymbol{\sigma}, \dot{\boldsymbol{\sigma}})$ to zero in finite-time.

The above problem is solved by a second-order sliding mode control (2-SMC). In particular, we are looking for a smooth version of such kind of controller, which means that the provided control input $\mathbf{u}$ has continuous time derivatives. Further, note that after concluding the objective of Problem 1, from Lemma 1, it is immediate to see that the system states $\mathbf{x}_1$ and $\mathbf{x}_2$ converge asymptotically to zero, thus realizing the desired position-attitude tracking.

3 Multi-Input Smooth 2-SMC

Using a reaching-law approach [11], the Problem 1 can be solved if the smooth control $\mathbf{u}$ turns the $\boldsymbol{\sigma}$-dynamics

$$\dot{\boldsymbol{\sigma}} = \mathbf{A}(\bar{\mathbf{x}}_1 - \mathbf{x}_1)\big[\mathbf{f}_2(\mathbf{x}_1,\mathbf{x}_2) + \mathbf{B}(\mathbf{x}_1)\mathbf{u} + \mathbf{G}(\mathbf{x}_1)\mathbf{d}\big] + \boldsymbol{\mathcal{C}}_{\boldsymbol{\sigma}}\mathbf{A}(\bar{\mathbf{x}}_1 - \mathbf{x}_1)\mathbf{x}_2 + \dot{\mathbf{A}}(\bar{\mathbf{x}}_1 - \mathbf{x}_1)\mathbf{x}_2, \tag{15}$$

in which $\bar{\mathbf{x}}_1 = \bar{\boldsymbol{\eta}}$, into the prescribed finite-time convergent dynamics

$$\begin{cases} \dot{\boldsymbol{\sigma}} = -\boldsymbol{\Gamma}_1\boldsymbol{\Psi}^{\frac{2}{3}}\mathrm{sign}(\boldsymbol{\sigma}) + \mathbf{w}, & (16)\\ \dot{\mathbf{w}} = -\boldsymbol{\Gamma}_2\boldsymbol{\Psi}^{\frac{1}{3}}\mathrm{sign}(\boldsymbol{\sigma}), & (17) \end{cases}$$

where $\boldsymbol{\Psi} \triangleq \mathrm{diag}(|\sigma_1|, \ldots, |\sigma_6|)$ and $\boldsymbol{\Gamma}_1 \in \mathbb{R}^{6\times 6}$, $\boldsymbol{\Gamma}_2 \in \mathbb{R}^{6\times 6}$ are positive diagonal matrices.

Lemma 2 ([17]). The dynamics (16)–(17) converges to zero in finite time, if and only if, it is asymptotically stable and its degree of homogeneity $q \in \mathbb{R}$ is negative.

Proof. The asymptotic stability of the origin can be proved by choosing the Lyapunov candidate function $V = \frac{1}{2}\mathbf{w}^{\mathrm{T}}\boldsymbol{\Gamma}_1\mathbf{w} + \frac{3}{4}\boldsymbol{\Gamma}_2\boldsymbol{\Psi}^{\frac{4}{3}}\mathbf{1}_6$, and subsequently applying the LaSalle's theorem to find that the only invariant set inside the set $\{\dot{V}(\boldsymbol{\sigma}, \mathbf{w})) = \mathbf{0}\}$ is the origin. Moreover, a vector field $\mathbf{f} : \mathbb{R}^n \to \mathbb{R}^n$ is called of homogeneous degree $q \in \mathbb{R}$ w.r.t. the dilation $d_k : (x_1, x_2, ..., x_n) \to (k^{m_1}x_1, k^{m_2}x_2, ..., k^{m_n}x_n)$, where $m_1, ..., m_n$ are positive number, if for any $k > 0$ the identity $\mathbf{f}(\mathbf{x}) = k^{-q}\mathbf{D}_k^{-1}\mathbf{f}(\mathbf{D}_k\mathbf{x})$, in which $\mathbf{D}_k \in \mathbb{R}^{n\times n} \triangleq \mathrm{diag}(k^{m1}, ..., k^{m_n})$, holds. It can be shown that the system (16)–(17) has a negative homogeneity degree $q = -1$ w.r.t. the dilation $d_k : (\boldsymbol{\sigma}^{\mathrm{T}}, \mathbf{w}^{\mathrm{T}}) \to (k^3\boldsymbol{\sigma}^{\mathrm{T}}, k^2\mathbf{w}^{\mathrm{T}})$ [16], and converges in finite time to the origin. □

Now, let us express $\mathbf{u} = \mathbf{u}_0 + \mathbf{u}_1$, with

$$\mathbf{u}_0 = -\mathbf{B}(\mathbf{x}_1)^{-1}\left(\mathbf{f}_2(\mathbf{x}_1,\mathbf{x}_2) + \mathbf{A}^{-1}(\bar{\mathbf{x}}_1 - \mathbf{x}_1)\boldsymbol{\mathcal{C}}_{\boldsymbol{\sigma}}\mathbf{A}(\bar{\mathbf{x}}_1 - \mathbf{x}_1)\mathbf{x}_2 + \mathbf{A}^{-1}(\bar{\mathbf{x}}_1 - \mathbf{x}_1)\dot{\mathbf{A}}(\bar{\mathbf{x}}_1 - \mathbf{x}_1)\mathbf{x}_2\right) \tag{18}$$

representing a smooth nominal control that cancels all the known quantities in the right-hand side of equation (15). Substituting equation (18) into (15), we obtain the $\boldsymbol{\sigma}$-dynamics in the form

$$\dot{\boldsymbol{\sigma}} = \mathbf{H}(\mathbf{x}_1)\mathbf{d} + \mathbf{N}(\mathbf{x}_1)\mathbf{u}_1, \tag{19}$$

where $\mathbf{H}(\mathbf{x}_1) \triangleq \mathbf{A}(\bar{\mathbf{x}}_1 - \mathbf{x}_1)\mathbf{G}(\mathbf{x}_1)$ and $\mathbf{N}(\mathbf{x}_1) \triangleq \mathbf{A}(\bar{\mathbf{x}}_1 - \mathbf{x}_1)\mathbf{B}(\mathbf{x}_1)$.

A control that provides $(\boldsymbol{\sigma}, \dot{\boldsymbol{\sigma}}) = (\mathbf{0}, \mathbf{0})$, has to satisfy the equality $\mathbf{u}_1 = \mathbf{N}(\mathbf{x}_1)^{-1}\mathbf{H}(\mathbf{x}_1)\mathbf{d}$. However, due to the problem uncertainties, any continuous and smooth feedback controller are not able to respect this equality. To get around this limitation, the disturbance is estimated by means of a special observer, which is presented further. The definition of $\mathbf{u}_1$ as

$$\begin{cases} \mathbf{u}_1 = \mathbf{N}(\mathbf{x}_1)^{-1}\left(-\boldsymbol{\Gamma}_1\boldsymbol{\Psi}^{\frac{2}{3}}\text{sign}(\boldsymbol{\sigma}) + \mathbf{w} - \mathbf{z}_1\right), & (20) \\ \dot{\mathbf{w}} = -\boldsymbol{\Gamma}_2\boldsymbol{\Psi}^{\frac{1}{3}}\text{sign}(\boldsymbol{\sigma}), & (21) \end{cases}$$

where $\mathbf{z}_1 \in \mathbb{R}^6$ is the observer output, results in the prescribed dynamics (16)–(17) and solves Problem 1, if and only if, $\mathbf{z}_1 \to \mathbf{H}(\mathbf{x}_1)\mathbf{d}$ in finite-time.

Using the definitions of $\mathbf{u}_0$ (18) and $\mathbf{u}_1$ (20), the designed controller is given by

$$\begin{aligned} \mathbf{u} = -\mathbf{B}(\mathbf{x}_1)^{-1}\Big(\mathbf{f}_2(\mathbf{x}_1,\mathbf{x}_2) + \mathbf{A}^{-1}(\bar{\mathbf{x}}_1 - \mathbf{x}_1)\boldsymbol{\mathcal{C}}_{\boldsymbol{\sigma}}\mathbf{A}(\bar{\mathbf{x}}_1 - \mathbf{x}_1)\mathbf{x}_2 + \mathbf{A}^{-1}(\bar{\mathbf{x}}_1 - \mathbf{x}_1)\dot{\mathbf{A}}(\bar{\mathbf{x}}_1 - \mathbf{x}_1)\mathbf{x}_2\Big) + ... \quad (22) \\ ... + \mathbf{N}(\mathbf{x}_1)^{-1}\left(-\boldsymbol{\Gamma}_1\boldsymbol{\Psi}^{\frac{2}{3}}\text{sign}(\boldsymbol{\sigma}) + \mathbf{w} - \mathbf{z}_1\right). \end{aligned}$$

Consider that the bounded disturbance $\mathbf{d}$ is one time differentiable and its continuous derivative $\dot{\mathbf{d}}$ have known Lipshitz constants $l_i, \forall i = 1, ..., 6$. The non-linear observer defined in Shtessel et al. [16] is expanded for the multi-input case to estimate $\mathbf{d}$ and $\dot{\mathbf{d}}$, being given by

$$\begin{cases} \dot{\mathbf{z}}_0 = \mathbf{v}_0 + \mathbf{N}(\mathbf{x}_1)\mathbf{u}_1, \\ \mathbf{v}_0 = -\boldsymbol{\Lambda}_0\mathbf{L}^{\frac{1}{3}}\boldsymbol{\mathcal{M}}(\mathbf{z}_0, \boldsymbol{\sigma})^{\frac{2}{3}}\text{sign}(\mathbf{z}_0 - \boldsymbol{\sigma}) + \mathbf{z}_1, \\ \dot{\mathbf{z}}_1 = \mathbf{v}_1, \\ \mathbf{v}_1 = -\boldsymbol{\Lambda}_1\mathbf{L}^{\frac{1}{2}}\boldsymbol{\mathcal{M}}(\mathbf{z}_1, \mathbf{v}_0)^{\frac{1}{2}}\text{sign}(\mathbf{z}_1 - \mathbf{v}_0) + \mathbf{z}_2, \\ \dot{\mathbf{z}}_2 = -\boldsymbol{\Lambda}_2\mathbf{L}\text{sign}(\mathbf{z}_2 - \mathbf{v}_1), \end{cases} \quad (23)$$

where $\boldsymbol{\mathcal{M}}(\mathbf{x}, \mathbf{y}) \triangleq \text{diag}(|x_1 - y_1|, ..., |x_6 - y_6|)$, $\mathbf{L} \triangleq \text{diag}(l_1, ..., l_6)$, and $\boldsymbol{\Lambda}_i \in \mathbb{R}^{6\times6}$, $\forall i = 0, 1, 2$, are diagonal matrices.

In the absence of input noises, the equalities

$$\begin{cases} \mathbf{z}_0 = \boldsymbol{\sigma}(t), \\ \mathbf{z}_1 = \mathbf{v}_0 \quad = \quad \mathbf{H}(\mathbf{x}_1)\mathbf{d}, \\ \mathbf{z}_2 = \mathbf{v}_1 = \frac{d}{dt}\left(\mathbf{H}(\mathbf{x}_1)\mathbf{d}\right), \end{cases} \quad (24)$$

are established in finite time [16], and are a sufficient condition to solve Problem 1.

4 Numerical Simulation

This section presents a computational simulation of the proposed method, coded in MATLAB script, where the proposed smooth 2-SMC is implemented in a full-actuated multirotor airship with a total mass $m = 9.58\,\text{kg}$. The hull has a length $L = 3.42\,\text{m}$, a maximum diameter $D = 1.80\,\text{m}$, and a volume $V = 5.8\,\text{m}^3$. The displacement between $\mathcal{S}_c$ and $\mathcal{S}_b$ is $\mathbf{r}_b^{c/b} = (0, 0, -0.67)\,\text{m}$. The simulation is performed with a time step of 0.001 s and uses the Euler integration method. The parameters of the observer and controller are shown in Table 1.

Table 1. Parameters of the controller and observer.

Description	Symbol	Value
Sliding surface coeff. matrix	$\boldsymbol{\mathcal{C}}_{\boldsymbol{\sigma}}$	$\mathbf{I}_6$
Smooth 2-SMC gain matrix	$\boldsymbol{\Gamma}_1$	diag (4, 2, 2, 0.5, 0.5, 0.5)
Smooth 2-SMC gain matrix	$\boldsymbol{\Gamma}_2$	diag (3, 1.5, 1.5, 0.5, 0.5, 0.5)
Observer Lipshitz constants matrix	$\mathbf{L}$	diag (160.52, 84.31, 80.22, 81.56, 53.45, 42.40)
Observer Lipshitz gain matrix	$\boldsymbol{\Lambda}_0$	diag (10, 10, 10, 5, 5, 5)
Observer Lipshitz gain matrix	$\boldsymbol{\Lambda}_1$	diag (6, 6, 6, 3, 3, 3)
Observer Lipshitz gain matrix	$\boldsymbol{\Lambda}_2$	diag (4, 4, 4, 2, 2, 2)

The observer Lipshitz constants matrix is calculated computationally.

The vehicle's mission is to reach the target point $\bar{\mathbf{r}}_g \triangleq (10, 2, 1.5)\,\mathrm{m}$ and the target attitude $\bar{\boldsymbol{\gamma}} \triangleq (0, 0, 8.75)$ deg, in ten seconds, with constant linear and angular velocities. In other words, ramp inputs are applied to the commanded position and heading and step inputs are applied to the commanded linear and angular velocities. The vehicle is hoovering in the initial time instant. Figures 2 and 3 show the simulation results.

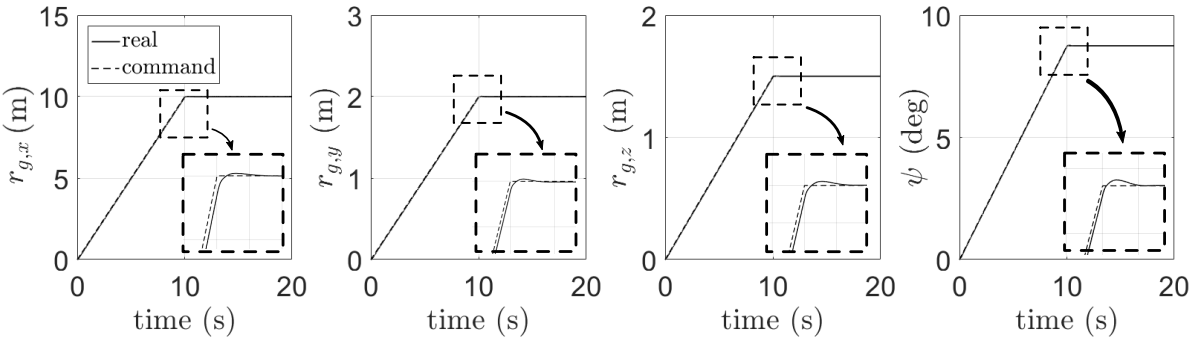

Figure 2. Real and commanded position/heading.

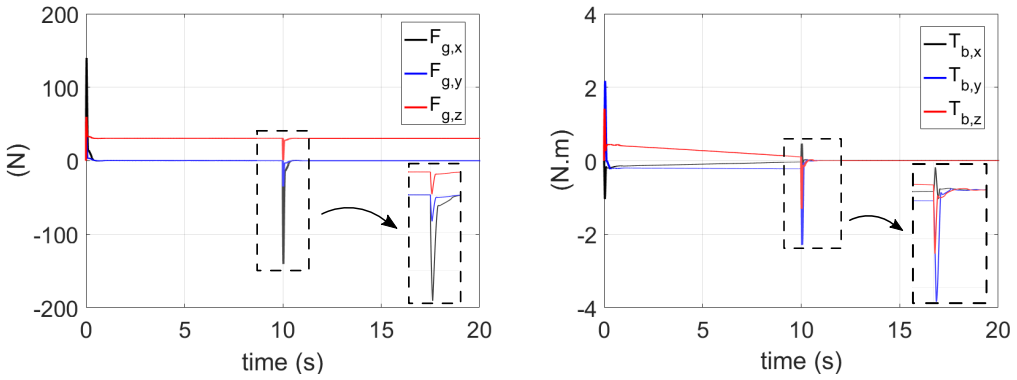

Figure 3. Control force and torque.

Figure 2 shows the effectiveness of the proposed smooth 2-SMC to control the full-actuated multirotor airship with non-modeled rotors dynamics, which means that the commanded and real control effort are the same, and unknown aerodynamic effects. Figure 3 presents the commanded control effort in each direction. The peaks observed at zero and ten seconds are due to the commanded velocities input profiles. The analysis of the control effort magnitude and direction serve as a reference to properly design the airframe rotors configuration in a future step of this study.

5 Conclusions

The paper proposed a multi-input smooth 2-SMC formulation to control the position and attitude of a full-actuated multirotor airship, subjected to unknown aerodynamic effects. The reaching mode finite-time convergence, is proved using homogeneity, and is assured by means of a special non-linear observer. A simulation example showed the effectiveness of the proposed method. In a future work, the proposed controller will be evaluated into the broader control problem, that encompass the control allocation into the rotors configuration and its subsequently application to the full vehicle's dynamics (including the rotors).

6 Acknowledgments

The authors would like to thank the Sao Paulo Research Foundation (FAPESP), for the financial support under grant 2019/05334-0. The first author is grateful to EMBRAER and ITA, for the doctorate

scholarship under the Academic-Industrial Graduate Program (DAI). The second author is also grateful for the support of the Brazilian National Council for Scientific and Technological Development (CNPq), under grant 302637/2018-4.

Authorship statement. The authors hereby confirm that they are the sole liable persons responsible for the authorship of this work, and that all material that has been herein included as part of the present paper is either the property (and authorship) of the authors, or has the permission of the owners to be included here.

References

[1] Saska, M., Chudoba, J., Přeučil, L., Thomas, J., Loianno, G., Třešňák, A., Vonásek, V., & Kumar, V., 2014. Autonomous deployment of swarms of micro-aerial vehicles in cooperative surveillance. In *2014 International Conference on Unmanned Aircraft Systems (ICUAS)*, pp. 584–595. IEEE.
[2] Air, A. P., 2016. First prime air delivery.
[3] Mogili, U. R. & Deepak, B. B. V. L., 2018. Review on Application of Drone Systems in Precision Agriculture. *Procedia Computer Science*, vol. 133, pp. 502–509.
[4] Santos, D. A. & Cunha Jr, A., 2017. Dynamic modeling and flight control of a balloon-quadcopter unmanned aerial vehicle. *XXXVIII Ibero-Latin American Congress on Computational Methods in Engineering*.
[5] Santos, D. A. & Cunha Jr, A., 2019. Flight control of a hexa-rotor airship: Uncertainty quantification for a range of temperature and pressure conditions. *ISA Transactions*, vol. 93, pp. 268 – 279.
[6] Ricardo Jr, J. A., 2020. Aerodynamic modeling of bluff hulls for flight control of small multi-rotor airships. Master's thesis, Aeronautics Institute of Technology.
[7] Drajunov, S. V. & Utkin, V. I., 1991. Sliding mode control in dynamic systems. *International Journal of Control*, pp. 1029–1037.
[8] Emelyanov, S. V., 1967. Variable structure control systems. *Moscow: Nauka*.
[9] Itkis, Y., 1976. Control systems of variable structure. *New York: Wiley*.
[10] Utkin, V., 1977. Variable structure systems with sliding modes. *IEEE Transactions on Automatic Control*.
[11] Hung, J. Y., Gao, W., & Hung, J. C., 1993. Variable structure control: a survey. *IEEE Transactions on Industrial Electronics*, vol. 40, n. 1, pp. 2–22.
[12] Lee, J. & Utkin, V., 2007. Chattering suppression methods in sliding mode control systems. *Annual Reviews in Control*, vol. 31, pp. 179–188.
[13] Levant, A., 2007. Principles of 2-sliding mode design. *Automatica*, vol. 43, n. 4, pp. 576–586.
[14] Bartolini, G., Ferrara, A., & Punta, E., 2000. Multi-input second-order sliding-mode hybrid control of constrained manipulator. *Dynamics and Control*, vol. 10, pp. 277–296.
[15] Khan, M., Goh, K., & Spurgeon, S., 2003. Second order sliding mode control of a diesel engine. *Asian Journal of Control*, vol. 5, pp. 614–619.
[16] Shtessel, Y. B., Shkolnikov, I. A., & Levant, A., 2007. Smooth second-order sliding modes: Missile guidance application. *Automatica*, vol. 43, n. 8, pp. 614–619.
[17] Bhat, S. P. & Bernstein, D. S., 1997. Finite-time stability of homogeneous systems. *Proceedings of the American Control*.